

CHARACTERIZATION OF A SAMPLE OF INTERMEDIATE-TYPE AGN. II. Host Bulge Properties and Black Hole Mass Estimates

Erika Benítez¹, Jairo Méndez-Abreu^{2,3}, Isaura Fuentes-Carrera⁴, Irene Cruz-González¹, Benoni
Martínez¹, Luis López-Martin^{2,3}, Elena Jiménez-Bailón¹, Vahram Chavushyan⁵, Jonathan
León-Tavares⁶

erika@astro.unam.mx

Received _____; accepted December 4 2012

¹Instituto de Astronomía, Universidad Nacional Autónoma de México, Apdo. Postal 70-264,
México D.F. 04510, México

²Instituto de Astrofísica de Canarias, 38200 La Laguna, Tenerife, Spain

³Departamento de Astrofísica, Universidad de La Laguna, E-38205 La Laguna, Tenerife, Spain

⁴Escuela Superior de Física y Matemáticas, Instituto Politécnico Nacional (ESFM-IPN), U.P.
Adolfo López Mateos, México D.F. 07730, México

⁵Instituto Nacional de Astrofísica, Óptica y Electrónica, Apdo. Postal 51-216, 72000 Puebla,
México

⁶Aalto University Metsähovi Radio Observatory, Metsähovintie 114, 02540, Kylmälä, Finland

ABSTRACT

We present a study of the host bulge properties and their relations with the black hole mass on a sample of 10 intermediate-type active galactic nuclei (AGN). Our sample consists mainly of early type spirals, four of them hosting a bar. For $70^{+10}_{-17}\%$ of the galaxies we have been able to determine the type of the bulge, and find that these objects probably harbor a pseudobulge or a combination of classical bulge/ pseudobulge, suggesting that pseudobulges might be frequent in intermediate-type AGN. In our sample, $50 \pm 14\%$ of the objects show double-peaked emission lines. Therefore, narrow double-peaked emission lines seem to be frequent in galaxies harboring a pseudobulge or a combination of classical bulge/ pseudobulge. Depending on the bulge type, we estimated the black hole mass using the corresponding $M_{BH} - \sigma^*$ relation and found them with a range of: $5.69 \pm 0.21 < \log M_{BH}^{\sigma^*} < 8.09 \pm 0.24$. **Comparing these $M_{BH}^{\sigma^*}$ values with masses derived from the FWHM of $H\beta$ and the continuum luminosity at 5100 \AA from their SDSS-DR7 spectra (M_{BH}) we find that eight out of ten ($80^{+7}_{-17}\%$) galaxies have black hole masses that are compatible within a factor of 3. This result would support that M_{BH} and $M_{BH}^{\sigma^*}$ are the same for intermediate-type AGN as has been found for type 1 AGN. However, when the type of the bulge is taken into account only 3 out of the 7 ($43^{+18}_{-15}\%$) objects of the sample have their $M_{BH}^{\sigma^*}$ and M_{BH} compatible within 3- σ errors. We also find that estimations based on the $M_{BH} - \sigma^*$ relation for pseudobulges are not compatible in $50 \pm 20\%$ of the objects.**

Subject headings: galaxies: active -galaxies: bulges - galaxies: photometry

1. Introduction

The connection between black hole mass (M_{BH}) and several properties of the host galaxy bulges have been a remarkable finding and have been extensively used in large samples of active galactic nuclei (AGN; see Ferrarese & Ford 2005, for a review). Among them, the so called $M_{\text{BH}} - \sigma_*$ relation (Ferrarese & Merritt 2000; Gebhardt et al. 2000), which relates the M_{BH} with the central stellar velocity dispersion of the galaxy (σ_*), has been demonstrated to be a reliable way to estimate M_{BH} . However, a recent work by Hu (2008, see also Greene et al. 2008) showed that the nature of the host galaxy bulge must be carefully considered before attempting any estimation of the M_{BH} . This is mainly due to the existence of a dichotomy in the properties and formation mechanisms of bulges (Wyse et al. 1997; Kormendy & Kennicutt 2004).

On one hand, the merger of small galaxies has been suggested as the main path for bulge formation (Kauffmann et al. 1993), which is supported by the homogeneous bulge stellar populations of the Milky Way and M31 (Zoccali et al. 2003; Stephens et al. 2003). Bulges formed in such mergers are termed *classical* bulges (CB) and are similar to low-luminosity ellipticals. Their light distribution is described by a de Vaucouleurs law (e.g., Andredakis et al. 1995). They are composed primarily by old Population II stars (Mehlert et al. 2003; Thomas et al. 2005), which have spheroidal or weakly triaxial distributions (Méndez-Abreu et al. 2010). Alternatively, bulges may form via internal secular processes (see Kormendy & Kennicutt 2004, for a review) such as bar-driven gas inflows, bending instabilities, and clump instabilities. Evidence for secular bulge (*pseudobulge*) formation includes the near-exponential bulge light profiles (Andredakis & Sanders 1994; Fisher & Drory 2008). Pseudobulges (PB) are dominated by Population I stars (Thomas & Davies 2006), they appear to have lower metallicity (Ganda et al. 2007) and lower α/Fe enhancement with respect to the big bulges of early-type galaxies (Morelli et al. 2008). They also show a clear correlation between bulge and disk scale-lengths (e.g., Méndez-Abreu et al. 2008a), substantial rotation (Kormendy & Kennicutt 2004), and

the presence of boxy-peanut shaped bulges (e.g., Méndez-Abreu et al. 2008b). In addition, Laurikainen et al. (2007) have demonstrated that pseudobulges are more prevalent among normal galaxies than classical bulges.

As previously mentioned, a common way to estimate the M_{BH} is through the $M_{\text{BH}}-\sigma_*$ relation: $\log(M_{\text{BH}}/M_{\odot}) = \alpha + \beta \log(\sigma_*/200)$. However, considering that pseudobulges have properties that lie between those of classical bulges and those of disks, the question arises whether M_{BH} masses should correlate differently with pseudobulge velocity dispersions. Hu (2008) investigated the $M_{\text{BH}}-\sigma_*$ relation for disk galaxies and found that it is different for pseudobulges over a 3σ significance level. Moreover, he noted that pseudobulges host smaller black holes than classical bulges do. One of his conclusions is that black holes (BH) form earlier than their host pseudobulges and that their growth is insignificant once the pseudobulges are formed. He also suggested that AGN fueling is less efficient in secular processes. Similar results were also found by Greene et al. (2008), Graham (2008), and Graham & Li (2009). However, other works performed by Beifiori et al. (2009) and Gültekin et al. (2009) did not find these differences. Recently, Kormendy et al. (2011) claimed that **nor pseudobulge luminosity, nor velocity dispersions of their hosts galaxies** correlate with M_{BH} mass since secular evolution processes lead to no coevolution of both components. Therefore, it is clear that when studying the M_{BH} it is important to know whether the central component is a classical bulge, a pseudobulge, or a mix of both.

In this work, we present new observations of a sample of 10 intermediate-type AGN using the Nordic Optical Telescope (NOT). We performed a careful morphological analysis of the sample, derived the surface-brightness profile for each galaxy and obtained their main structural parameters. In particular, we derived the Sérsic index, which along with other criteria, we used to establish the nature of each bulge, and then estimated the M_{BH} for all objects using different correlations according to the nature of the bulge. These mass estimates were also compared with

BH masses, M_{BH} derived in Benítez et al. (2012, hereafter Paper I) using SDSS-DR7 spectra and the relation given by Vestergaard & Peterson (2006). Differences and similitudes were analysed in the light of the nature of the bulge. In addition, in Paper I narrow double-peaked AGN were detected in five galaxies of the sample. This result is used in order to compare the nature of the bulges with the presence of single- or double-peaked emission lines in intermediate-type AGN.

The paper is organized as follows: Sect. 2 describes the observations and data reduction process. The host galaxy photometric decomposition and the galaxy structural parameters are explained in Sect. 3. The results obtained for the complete sample and for the individual objects are shown in Sect. 4. The discussion and conclusions are given in Sect. 5. The cosmology adopted in this work is $H_0 = 70 \text{ km s}^{-1} \text{ Mpc}^{-1}$, $\Omega_m = 0.3$ and $\Omega_\Lambda = 0.7$.

2. Observations and Data Reduction

The photometric observations were carried out using the ALFOSC instrument mounted at the 2.56-m NOT telescope at La Palma. We obtain deep and high quality *R*-band images using the 2048×2048 back-illuminated CCD with a plate scale of $0.19 \text{ arcsec pixel}^{-1}$ and $6.5 \times 6.5 \text{ arcmin}^2$ field of view. The observations were carried out during three runs (October 2006, April and May 2007). In Table 1 we present the list of observed objects and other observational details. The exposure times were chosen to keep counts in the detector linearity regime, and to avoid saturation in the bright central parts of the galaxies to resolve the different structures present in the galaxies. Data reduction was made in the standard way using IRAF¹. The bias subtraction was done using

¹IRAF is distributed by the National Optical Astronomy Observatories, operated by the Association of Universities for Research in Astronomy, Inc., under cooperative agreement with the National Science Foundation.

a master bias obtained at the beginning of the night. Flat-field corrections were applied using sky flats. We have used our own script to automatize the alignment of the images and removing cosmic rays at the same time. Night conditions were clear in general, and 2 nights (April 21st and May 11th, 2007) were strictly photometric. Figure 1 shows a mosaic with the *R*-band images for our sample objects.

3. Galaxy Photometric Decompositions

The structural parameters of the sample galaxies were derived by applying a two-dimensional photometric decomposition to the galaxy images. To this aim, the GASP2D algorithm developed by Méndez-Abreu et al. (2008a) was used. For the sake of clarity, and because some specific modifications have been done to the code, we will briefly describe here the main characteristics of GASP2D. The galaxy surface-brightness distribution (SBD) was assumed to be the sum of different components depending on the morphological features of each galaxy. The structural components considered in the decomposition were the following:

The Sérsic law (Sérsic 1963, 1968), also known as the $r^{1/n}$ law or generalized de Vaucouleurs law, was adopted to describe the surface brightness of the bulge component

$$I_{\text{bulge}}(r_{\text{bulge}}) = I_e 10^{-b_n \left[\left(\frac{r_{\text{bulge}}}{r_e} \right)^{\frac{1}{n}} - 1 \right]}, \quad (1)$$

where r_{bulge} is the radius measured in the Cartesian coordinates describing the reference system of the bulge in the plane of the sky. r_e , I_e , and n are the effective (or half-light) radius, the surface brightness at r_e , and a shape parameter describing the curvature of the SBD, respectively, and $b_n = 2n - 0.33$ (Caon et al. 1993).

The bulge isophotes are ellipses centered on the galaxy center (x_0, y_0) , with constant position angle PA_{bulge} and constant axial ratio q_{bulge} .

The SBD of the disk component was assumed to follow an exponential law (Freeman 1970)

$$I_{\text{disk}}(r_{\text{disk}}) = I_0 e^{-\left(\frac{r_{\text{disk}}}{h}\right)}, \quad (2)$$

where I_0 and h are the central surface brightness and scale-length of the disk, respectively. The disk isophotes are ellipses centered on (x_0, y_0) , with constant position angle PA_{disk} and constant axial ratio q_{disk} .

The projected surface density of a three-dimensional Ferrers ellipsoid (Ferrers 1877, see also Aguerri et al. 2009) was used to describe the SBD of bars

$$I_{\text{bar}}(r_{\text{bar}}) = I_{0,\text{bar}} \left[1 - \left(\frac{r_{\text{bar}}}{a_{\text{bar}}} \right)^2 \right]^{n_{\text{bar}}+0.5}; \quad r_{\text{bar}} \leq a_{\text{bar}}, \quad (3)$$

where $I_{0,\text{bar}}$, a_{bar} and n_{bar} represent the central surface brightness, length and shape parameter of the bar, respectively. Due to the high degree of degeneracy that the n_{bar} parameter introduces during the fit, we decided to keep it as a fixed parameter during the fitting process. The default value used was $n_{\text{bar}} = 2$ (see Laurikainen et al. 2005). All the bar models were built up in a frame of generalized ellipses (Athanasoula et al. 1990). Thus, the bar reference system is defined as

$$r_{\text{bar}} = \left[\frac{[(-(x - x_0) \sin \text{PA}_{\text{bar}} + (y - y_0) \cos \text{PA}_{\text{bar}})^c - ((x - x_0) \cos \text{PA}_{\text{bar}} + (y - y_0) \sin \text{PA}_{\text{bar}})^c]}{q_{\text{bar}}^c} \right]^{1/c}, \quad (4)$$

where q_{bar} and PA_{bar} are the axis ratio and position angle of the bar, respectively. The parameter c controls the shape of the isophotes. A value of $c = 2$ corresponds to a perfect ellipse, $c > 2$ to a boxy shape and $c < 2$ to a disky shape.

Since the central SBD of our objects is affected by the presence of an AGN, we have modeled its contribution, $I_{\text{NC}}(r_{\text{NC}})$, by means of a intensity scaled point spread function (PSF).

To derive the photometric parameters of the different components we fitted iteratively a model of the surface brightness

$$I_{\text{model}}(r) = I_{\text{bulge}}(r_{\text{bulge}}) + I_{\text{disk}}(r_{\text{disk}}) + I_{\text{bar}}(r_{\text{bar}}) + I_{\text{NC}}(r_{\text{NC}}), \quad (5)$$

to the pixels of the galaxy image, using a non-linear least-squares minimization based on a robust Levenberg-Marquardt method. The actual computation has been done using the MPFIT² algorithm implemented by C. B. Markwardt under the IDL³ environment. Each image pixel has been weighted according to the variance of its total observed photon counts due to the contribution of both the galaxy and sky, and determined assuming photon noise limitation and taking into account for the detector readout noise. The seeing effects were taken into account by convolving the model image with a circular Moffat PSF with the FWHM measured from stars in the galaxy image.

For each galaxy, a model was fitted to the SBD considering a central point-like component, a bulge, a bar and a disk component. Figures 2 to 11 show the GASP2D fits for each galaxy in the sample. The parameters derived for the structural components, together with the χ^2 values of the fits, are collected in Table 2.

The formal errors obtained from the χ^2 minimization procedure are usually not representative of the real errors in the structural parameters (Méndez-Abreu et al. 2008a). Therefore, the errors given in Table 2 were obtained through a series of Monte Carlo simulations. A set of 500 images of galaxies with a Sérsic bulge, an exponential disk, and a central PSF was generated. An analogue set including the bar component was also created. The structural parameters of the artificial galaxies were randomly chosen among the ranges obtained for our sample galaxies (see Table 2).

²The updated version of this code is available on <http://cow.physics.wisc.edu/craigm/idl/idl.html>

³Interactive Data Language

The simulated galaxies were assumed to be at a distance of 261 Mpc, which corresponds to the mean of our galaxy sample. The adopted pixel scale, CCD gain, and read-out-noise were chosen to mimic the instrumental setup of the photometric observations. Finally, a background level and photon noise were added to the artificial images to yield a signal-to-noise ratio similar to that of the observed ones. The images of artificial galaxies were analysed with GASP2D as if they were real. The errors on the fitted parameters were estimated by comparing the input and measured values assuming they were normally distributed. The mean and standard deviation of the relative errors of the artificial galaxies were adopted as the systematic and typical errors for the observed galaxies.

Another source of uncertainty in this study is the PSF mismatch. This issue becomes crucial in this study since our modelling requires the assumption of a given PSF to perform the image convolution and to describe the AGN component. To get rid of the PSF mismatch errors we have performed two different tests. First, we have repeated ten times the fit for every galaxy allowing the FWHM of the moffat function to vary within 5%. Second, we have also used a gaussian function with 5% variation of the FWHM. From the observed stars in the field, we found that the gaussian function is clearly a bad representation of the PSF, however we consider these errors as an upper limit of the variation in the structural parameters due to the PSF mismatch. The final errors shown in Table 2 represent the combination in quadrature of the Monte Carlo errors derived previously and the errors due to PSF mismatch.

The reader is referred to the individual galaxy description presented in Sect. 4, where details on the morphology obtained from NED⁴ and/or derived in this work, together with a discussion on the possible host bulge characterization (classical bulge or pseudobulge) are provided.

⁴The NASA/IPAC Extragalactic Database (NED) is operated by the Jet Propulsion Laboratory, California Institute of Technology, under contract with the National Aeronautics and Space Administration.

4. Results

4.1. Classical versus pseudobulges

The two-dimensional photometric decompositions performed on deep R -band images allowed us to determine the nature of the bulge of each galaxy. We separated classical bulges from pseudobulges using the prescriptions given by Kormendy & Kennicutt (2004). The more these characteristics apply, the safer the classification of pseudobulge becomes. Among these characteristics we use the analysis of the SBD of each galaxy, the value of the Sérsic index (usually bulges with $n < 2$ are considered pseudobulges; Fisher & Drory 2008), the ellipticities of the bulge and disk, the central stellar velocity dispersion (σ_*), and by the presence, or absence, of central structures from the inspection of the R -band residuals derived using the best fit. Four galaxies in our sample, #3, #4, #5 and #7, seem to harbor a pseudobulge, while for galaxies #1, #2 and #6, our analysis suggests a combination of a classical bulge and a pseudobulge. For galaxies #9 and #10, the photometric decomposition did not allow us to determine their Sérsic index, so we decided not to classify the nature of the bulge from this decomposition. Finally, galaxy #8 seems to be a merger, and with the available data we could not derive a value for the Sérsic index, therefore we cannot establish its bulge nature. In summary, we found that $70\%^{+10.1\%}_{-16.9\%}$ of the objects harbor pseudobulges or a combination of classical bulge/pseudobulge, which suggests that pseudobulges might be frequent in intermediate-type AGN. **In Paper I, double-peaked narrow emission lines were detected in the following intermediate-type AGN: #1, #3, #4, #5, and #8. In this work, we could establish the nature of the bulge in four of them, with the exception of object #8, and found that they harbor either a pseudobulge (#3, #4 and #5) or a mix of both bulge-types (CB/PB for object #1).** Our morphological classification also shows that most objects are early-type spirals, and our deep images allowed us to detect the presence of a bar in four of them. In the following section, we will explain in detail the main properties of the individual galaxies.

4.2. Notes on individual galaxies

4.2.1. *J120655.63+501737.1* (#1)

The SBD fit of this galaxy is presented in Fig. 2. It shows the presence of a 5.4 kpc bar. The host galaxy probably presents a combination of a classical bulge/pseudobulge, since the photometric decomposition provides us with a Sérsic index $n=2.8\pm1.2$. This n corresponds to a classical bulge (Kormendy & Kennicutt 2004), but considering the errors it could also be a pseudobulge. We cannot rule out a pseudobulge in this galaxy since the velocity dispersion ($\sigma_{\star}\sim 90 \text{ km s}^{-1}$) is small and the galaxy has a large bar. Both properties suggest the presence of a more rotationally supported component, usually associated to a pseudobulge. We note that this object has the largest Sérsic index value in the sample. The morphological type of this galaxy is T=2.9 (close to Sb) in the HyperLeda database ⁵. Since we found a bar component, we classify it as SBb.

4.2.2. *J121600.04+124114.3* (#2)

The SBD decomposition (see Fig. 3) suggests a classical bulge for this galaxy, which is supported by the absence of a bar, and the different ellipticities of the bulge and disk components. The Sérsic index $n=1.8\pm0.6$ favors a pseudobulge (**though** its scatter is large) **and the central velocity dispersion value is rather small** ($\sigma_{\star}\sim 110 \text{ km s}^{-1}$). This almost face-on galaxy is classified as Sb(r) in the NED database. Its spiral arms are particularly clumpy in the inner parts (within the central $5''\sim 4 \text{ kpc}$) and become very diffuse towards the edge of the galaxy, the northern outer arm stretches out to the east.

⁵<http://HyperLeda.univ-lyon1.fr>

4.2.3. *J121607.08+504930.0 (#3)*

This galaxy probably hosts a pseudobulge. The obtained bulge Sérsic index is $n=1.6\pm0.5$, and the similarity between the bulge and disk ellipticities ($\epsilon \sim 0.66$) along with the presence of a strong dust lane (see Fig. 4), indicates the presence of a rotating component in the central region of the galaxy. This galaxy is classified as a probable SBb in the NED database. However, our SBD fit shows no indication of a bar. Thus, we have re-classified this galaxy as an Sb.

4.2.4. *J141238.14+391836.5 (#4)*

The SBD analysis yields a bulge Sérsic index $n=1.4\pm0.8$. The bulge is flat with an ellipticity similar to that of the disk, both indicative of a pseudobulge. The presence of a pseudobulge is strengthened by the central spiral arms shown in the residual image of the SBD decomposition (see Fig. 5). However, we note that the central velocity dispersion ($\sigma_{\star} \sim \mathbf{195 \text{ km s}^{-1}}$) is somewhat large for a pseudobulge. This galaxy is classified as Sab in both NED and HyperLeda databases. We found no indication of the presence of a bar in this galaxy.

4.2.5. *J143031.18+524225.8 (#5)*

The SBD fit indicates that this galaxy hosts probably a pseudobulge. The bulge Sérsic index $n=1.3\pm0.6$, together with the similarity in bulge and disk ellipticities ($\epsilon \sim 0.36$), and the presence of a large bar ($a_{bar}=7.0$ kpc and $h=4.7$ kpc), reinforce the idea of secular processes acting in this galaxy. The galaxy has two spiral arms that are barely seen in broad-band images (see Fig. 6). These arms are well outlined and clumpy in $H\alpha$ images by Weistrop et al. (1995), especially the northern one. Considering the presence of the bar and the shape of the arms traced by $H\alpha$, this galaxy could be classified as an SBa-SBab galaxy.

4.2.6. *J144049.35+505009.2 (#6)*

For this galaxy, the SBD decomposition was done including a small bar ($a_{bar}=2.8$ kpc) but large uncertainties were obtained. Our analysis shows that this galaxy harbors both a classical bulge and a pseudobulge. The Sérsic index obtained is $n=1.6\pm0.8$ but compatible within the errors with values >2 . The bulge ellipticity indicates that it is flat. However, the presence of a central small bar might be contaminating this result, as can be seen in the galaxy ellipticity profile (see Fig. 7). Two very faint spiral arms are seen in the NOT R -band image over a faint disk and an elongation is seen to the south of the bulge. The inspection of the R -band image indicates this could be an early-type spiral. So, the morphological type is SBa.

4.2.7. *J153810.05+573613.1 (#7)*

The SBD decomposition shows that this galaxy hosts a pseudobulge, with a Sérsic index $n=1.6\pm0.3$. The central velocity dispersion is rather low ($\sigma_{\star} \sim \mathbf{91\ km\ s^{-1}}$). From Fig. 8 we note that there are hints favoring the presence of central substructures. Therefore, this galaxy probably hosts a pseudobulge. It is classified as Sc in NED since it displays open and flocculent spiral arms.

4.2.8. *J162952.88+242638.3 (#8)*

The SBD fit obtained for this galaxy must be taken with care since this object is probably an on-going merger (see Fig. 9). Since the morphology is disturbed and the light profile is not well fitted with an elliptically averaged $r^{1/n}$ model, we classify this galaxy as Peculiar. For this reason, the M_{BH} mass was estimated considering both possibilities: classical bulge and a pseudobulge.

4.2.9. *J212851.19-010412.4 (#9)*

The effective radius of the bulge obtained for this galaxy always converges to a minimum value equal to the PSF. Thus, Fig. 10 shows the best fit achieved considering a bright central component and a bulgeless galaxy. Since the Sérsic index cannot be determined, it is uncertain whether it harbors a classical bulge or a pseudobulge. We found no morphological classification for this galaxy in NED, nor in the HyperLeda database. Inspection of the NOT *R*-band image shows that it is a spiral galaxy seen almost face-on. From this image, it is not clear if the bulge is large and boxy, nor if it harbors a bar. The spiral arms are a bit flocculent. The eastern arm of the galaxy is brighter than its central parts-, then it becomes very diffuse and seems to bifurcate. For the western side of the galaxy, two very similar arms seem to emerge from the disk. Considering their degree of tightness, we classify this galaxy as an Sab.

4.2.10. *J234428.81+134946.0 (#10)*

For this galaxy, the SBD decomposition includes a 9.9 kpc bar and a disk with $h = 5.1$ kpc, but the bulge cannot be resolved since its effective radius always converges to a minimum value equal to the PSF. For this reason, the value for the Sérsic index cannot be determined, nor whether it has a classical bulge or a pseudobulge. This galaxy has a de Vaucouleurs' type of 4.1 ± 5.0 in the HyperLEDA database. This corresponds to a morphological type of Sbc, though the error does not allow a precise classification. According to our NOT image and the SBD decomposition (see Fig. 11), this is a barred galaxy. Arms are very faint, tight and flocculent. A very faint arm is seen in the northern part extending to the north-west. We classify this galaxy as a SBab.

4.3. M_{BH} estimates

Using the σ_* calculated in Paper I, we obtained **the BH mass** using either the $M_{BH}-\sigma_*$ relation given by Ferrarese & Ford (2005) for classical bulges ($\alpha = 8.06 \pm 0.67$, $\beta = 4.86 \pm 0.43$) or **the one given by** Hu (2008), ($\alpha = 7.50 \pm 0.18$, $\beta = 4.5 \pm 1.3$) for pseudobulges. In the cases where the bulges are probably a combination of both classical and pseudobulge (CB/PB) we estimated the $M_{BH}^{\sigma_*}$ using both correlations. The results of these $M_{BH}^{\sigma_*}$ estimations are given in Table 3, see Col(4) and (5). Also in this table the **BH** mass estimates (M_{BH}) obtained in Paper I are presented in Col (6). The $M_{BH}^{\sigma_*}$ has a range of **$5.69 \pm 0.21 < \log M_{BH}^{\sigma_*} < 8.09 \pm 0.24$** .

Figure 12 shows the comparison between the $M_{BH}^{\sigma_*}$ masses obtained depending on the nature of the bulge with the M_{BH} **estimated in Paper I. In this figure, we have marked in the upper and lower panels a region defined by dotted lines that corresponds to 3 and 1/3 times the $M_{BH} = M_{BH}^{\sigma_*}$ relation. In the upper panel we show our results for seven out of ten galaxies that we have found harbor a PB or a mix of both, i.e. CB/PB. We also show the estimations obtained for the other three galaxies that still have unknown bulge type assuming that they could harbor a PB. From this panel, we see that object #8 lies well within the dotted lines, object #10 lies marginally but object #9 clearly lies out. Now, considering only the objects with bulge-type found in this work, we find that objects #4, #5 and #6 fall inside the dotted region. The remaining four objects #1,#2,#3 and #7 are out of the dotted region. Furthermore, in the lower panel we show the estimates obtained for objects that were found to harbor a mix of CB/PB, i.e. #1, #2 and #6. In this case, $M_{BH}^{\sigma_*}$ was estimated using Ferrarese & Ford (2005). It is interesting to note that two of them lie marginally inside the dotted region and one lies completely out of it (#6). Regarding the three unknown bulge-type objects, we see that object #10 lies inside the dotted region, object #9 could be considered a marginal case and object #8 lies out of the region.**

5. Discussion and conclusions

In this paper, we derived the R-band host-bulge structural parameters of a sample of 10 intermediate-type AGN. Through a detailed two-dimensional photometric decomposition analysis we find that most of the host galaxies are early-type spirals and four of them have a bar. This analysis, together **with a careful morphological analysis** and the velocity dispersion obtained in Paper 1, **allowed us to determine the nature of the bulge in seven out of ten intermediate-type AGN. In these seven objects, we find that all of them harbor a pseudobulge or a combination of both bulge-types (CB/PB). To our knowledge, this is the first time that such a detailed study on the nature of the bulge-type is done to a sample of intermediate-type AGN. Although the sample is not extensive, our work strongly suggests that pseudobulges are actually frequent in this class of objects.**

In Paper I, we suggested that intermediate-type AGN should be analyzed separately from Type 1 or 2 AGN due to the high fraction of narrow double-peaked sources found in our sample ($50\% \pm 14.4\%$). In this work, we have also find that narrow double-peaked emission lines are more frequently found in galaxies harboring a pseudobulge or a combination of classical bulge/pseudobulge (four out of **seven galaxies with bulge classification are double-peaked, $57\%^{+14.9\%}_{-18.1\%}$ harbor a PB or CB/PB).**

On the basis of the bulge nature, we calculated $M_{BH}^{\sigma\star}$ using the empirical relation given by Hu (2008) for pseudobulges, and also the relation given by Ferrarese & Ford (2005) for classical bulges **when the bulge-type resulted to be a mix of both. We have also used the M_{BH} estimations given in Paper 1 that were obtained with the scaling relations given by Vestergaard & Peterson (2006). The black hole mass range obtained with the three methods is $5.69 \pm 0.21 < \log M_{BH} < 8.09 \pm 0.24$. The three tested methods yield no systematically different results for the range of masses: the range for classical bulges is $6.26 \pm 0.04 < \log M_{BH}^{\sigma\star} < 8.09 \pm 0.24$; for pseudobulges $5.69 \pm 0.21 < \log M_{BH}^{\sigma\star} < 7.38 \pm 0.32$; and with the scaling**

relations yields $6.54 \pm 0.16 < \log M_{BH} < 7.81 \pm 0.14$. It should be noted that, since we have showed that pseudobulges are frequent in intermediate type-AGN, and taken into account that the $M_{BH} - \sigma^*$ relation for classical bulges gives systematically higher masses than the one for pseudobulges, in principle one should use the pseudobulge $M_{BH} - \sigma^*$ relation in order to not overestimate the black hole mass.

However, comparing our $M_{BH}^{\sigma^*}$ estimates with the M_{BH} obtained using the scaling relations, we find that only four out of the ten ($40^{+16}_{-13}\%$) galaxies (#5, #6, #8 and #10) are compatible within $1-\sigma$ errors and one more (#4) is compatible within $3-\sigma$ (that is, $50 \pm 20\%$ in total). Peterson (2012) advised that black hole mass estimations using the scaling relations can be reliable within a factor of ~ 3 . When this criterium is applied, the masses obtained with $M_{BH}^{\sigma^*}$ relations and M_{BH} are compatible for eight (all except #3 and #7) of the galaxies in the sample ($80^{+7}_{-17}\%$). If this criterium is valid for our sample, our results show that the scaling relations derived from Type 1 AGN (e.g., Woo et al. 2010; Bennert et al. 2011) are the same for intermediate-type AGN.

From our seven classified bulges we could specify that four of them ($57^{+15}_{-18}\%$) harbor certainly pseudobulges (#3, #4, #5, #7). For these, only half ($50 \pm 20\%$) of them (#4 and #5) present masses compatible within $3-\sigma$ for both methods (upper panel figure 12). The same result is obtained when the factor-3 criterium in the mass determination is applied. The remaining three galaxies (#1, #2 and #6) are compatible with both bulge types being classical and pseudobulge. Assuming that these three objects do harbor a pseudobulge, only one out three (#6) presents compatible masses considering both the $3-\sigma$ and the factor-3 criteria. On the other hand, considering them as classical bulges, we find that none have compatible masses within $3-\sigma$ errors, but two of them (#1 and #2) do actually have compatible masses if the factor-3 criterium is applied (lower panel figure 12).

In summary, when the type of the bulge is taken into account, only three (depending

on both things: the criterium applied to the uncertainties and the type of bulge for the CB/PB galaxies) out of the seven ($43^{+18}_{-15}\%$) galaxies of the sample have compatible $M_{BH}^{\sigma*}$ and M_{BH} . Nothing can be concluded for galaxies #8, #9 and #10 since the nature of their bulge is unknown. We also find that the black hole mass estimates based on the $M_{BH} - \sigma^*$ relation for pseudobulges is not compatible in $50 \pm 20\%$ of the objects. Therefore, these objects would support the result found by Kormendy et al. (2011) since their velocity dispersion does not correlate with the black hole mass. However, our results are based on a small number of objects, and therefore we stress the importance to perform similar detailed analysis in which the type of bulge can be determine using larger samples.

We want to thank the anonymous referee for useful comments and suggestions. We also thank Dr. D. Clark who carefully read the final version of the manuscript. EB acknowledges financial support from UNAM-DGAPA-PAPIIT through grant IN116211. JMA is partially funded by the Spanish MICINN under the Consolider-Ingenio 2010 Program grant CSD2006-00070 and also by the grants AYA2007-67965-C03-01 and AYA2010-21887-C04-04. IFC thanks the financial support from CONACYT grant 0133520 and IPN-SIP grant 20121700. The data presented here were obtained with ALFOSC, which is provided by the Instituto de Astrofísica de Andalucía (IAA) under a joint agreement with the University of Copenhagen and NOTSA. Funding for the SDSS and SDSS-II has been provided by the Alfred P. Sloan Foundation, the Participating Institutions, the National Science Foundation, the U.S. Department of Energy, the National Aeronautics and Space Administration, the Japanese Monbukagakusho, the Max Planck Society, and the Higher Education Funding Council for England. The SDSS Web Site is <http://www.sdss.org/>. This research has made use of the NASA/IPAC Extragalactic Database (NED) which is operated by the Jet Propulsion Laboratory, California Institute of Technology, under contract with the National Aeronautics and Space Administration. We acknowledge the usage of the HyperLeda database (<http://leda.univ-lyon1.fr>).

REFERENCES

- Aguerri, J. A. L., Méndez-Abreu, J., & Corsini, E. M. 2009, *A&A*, 495, 491
- Andredakis, Y. C., Peletier, R. F., & Balcells, M. 1995, *MNRAS*, 275, 874
- Andredakis, Y. C. & Sanders, R. H. 1994, *MNRAS*, 267, 283
- Athanassoula, E., Morin, S., Wozniak, H., Puy, D., Pierce, M. J., Lombard, J., & Bosma, A. 1990, *MNRAS*, 245, 130
- Beifiori, A., Sarzi, M., Corsini, E. M., Dalla Bontà, E., Pizzella, A., Coccato, L., & Bertola, F. 2009, *ApJ*, 692, 856
- Bennert, V. N., Auger, M. W., Treu, T., Woo, J.-H., & Malkan, M. A. 2011, *ApJ*, 726, 59
- Caon, N., Capaccioli, M., & D’Onofrio, M. 1993, *MNRAS*, 265, 1013
- Ferrarese, L. & Ford, H. 2005, *Space Sci. Rev.*, 116, 523
- Ferrarese, L. & Merritt, D. 2000, *ApJ*, 539, L9
- Ferrers, N. M. 1877, *Quart. J. Pure Appl. Math.*, 14, 1
- Fisher, D. B. & Drory, N. 2008, *AJ*, 136, 773
- Freeman, K. C. 1970, *ApJ*, 160, 811
- Ganda, K., Peletier, R. F., McDermid, R. M., Falcón-Barroso, J., de Zeeuw, P. T., Bacon, R., Cappellari, M., Davies, R. L., Emsellem, E., Krajnović, D., Kuntschner, H., Sarzi, M., & van de Ven, G. 2007, *MNRAS*, 380, 506
- Gebhardt, K., Bender, R., Bower, G., Dressler, A., Faber, S. M., Filippenko, A. V., Green, R., Grillmair, C., Ho, L. C., Kormendy, J., Lauer, T. R., Magorrian, J., Pinkney, J., Richstone, D., & Tremaine, S. 2000, *ApJ*, 539, L13

- Graham, A. W. 2008, *ApJ*, 680, 143
- Graham, A. W. & Li, I.-h. 2009, *ApJ*, 698, 812
- Greene, J. E., Ho, L. C., & Barth, A. J. 2008, *ApJ*, 688, 159
- Gültekin, K., Richstone, D. O., Gebhardt, K., Lauer, T. R., Tremaine, S., Aller, M. C., Bender, R., Dressler, A., Faber, S. M., Filippenko, A. V., Green, R., Ho, L. C., Kormendy, J., Magorrian, J., Pinkney, J., & Siopis, C. 2009, *ApJ*, 698, 198
- Hu, J. 2008, *MNRAS*, 386, 2242
- Kauffmann, G., White, S. D. M., & Guiderdoni, B. 1993, *MNRAS*, 264, 201
- Kormendy, J., Bender, R., & Cornell, M. E. 2011, *Nature*, 469, 374
- Kormendy, J. & Kennicutt, Jr., R. C. 2004, *ARA&A*, 42, 603
- Laurikainen, E., Salo, H., & Buta, R. 2005, *MNRAS*, 362, 1319
- Laurikainen, E., Salo, H., Buta, R., & Knapen, J. H. 2007, *MNRAS*, 381, 401
- Mehlert, D., Thomas, D., Saglia, R. P., Bender, R., & Wegner, G. 2003, *A&A*, 407, 423
- Méndez-Abreu, J., Aguerri, J. A. L., Corsini, E. M., & Simonneau, E. 2008a, *A&A*, 478, 353
- Méndez-Abreu, J., Corsini, E. M., Debattista, V. P., De Rijcke, S., Aguerri, J. A. L., & Pizzella, A. 2008b, *ApJ*, 679, L73
- Méndez-Abreu, J., Simonneau, E., Aguerri, J. A. L., & Corsini, E. M. 2010, *A&A*, 521, A71+
- Morelli, L., Pompei, E., Pizzella, A., Méndez-Abreu, J., Corsini, E. M., Coccato, L., Saglia, R. P., Sarzi, M., & Bertola, F. 2008, *MNRAS*, 389, 341
- Peterson, B. M. 2012, *Journal of Physics Conference Series*, 372, 012008

- Sérsic, J. L. 1963, *Boletín de la Asociación Argentina de Astronomía La Plata Argentina*, 6, 41
- . 1968, *Atlas de galaxias australes* (Cordoba, Argentina: Observatorio Astronómico, 1968)
- Stephens, A. W., Frogel, J. A., DePoy, D. L., Freedman, W., Gallart, C., Jablonka, P., Renzini, A., Rich, R. M., & Davies, R. 2003, *AJ*, 125, 2473
- Thomas, D. & Davies, R. L. 2006, *MNRAS*, 366, 510
- Thomas, D., Maraston, C., Bender, R., & Mendes de Oliveira, C. 2005, *ApJ*, 621, 673
- Vestergaard, M. & Peterson, B. M. 2006, *ApJ*, 641, 689
- Weistrop, D., Hintzen, P., Liu, C., Lowenthal, J., Cheng, K., Oliversen, R., Brown, L., & Woodgate, B. 1995, *AJ*, 109, 981
- Woo, J.-H., Treu, T., Barth, A. J., Wright, S. A., Walsh, J. L., Bentz, M. C., Martini, P., Bennert, V. N., Canalizo, G., Filippenko, A. V., Gates, E., Greene, J., Li, W., Malkan, M. A., Stern, D., & Minezaki, T. 2010, *ApJ*, 716, 269
- Wyse, R. F. G., Gilmore, G., & Franx, M. 1997, *ARA&A*, 35, 637
- Zoccali, M., Renzini, A., Ortolani, S., Greggio, L., Saviane, I., Cassisi, S., Rejkuba, M., Barbuy, B., Rich, R. M., & Bica, E. 2003, *A&A*, 399, 931

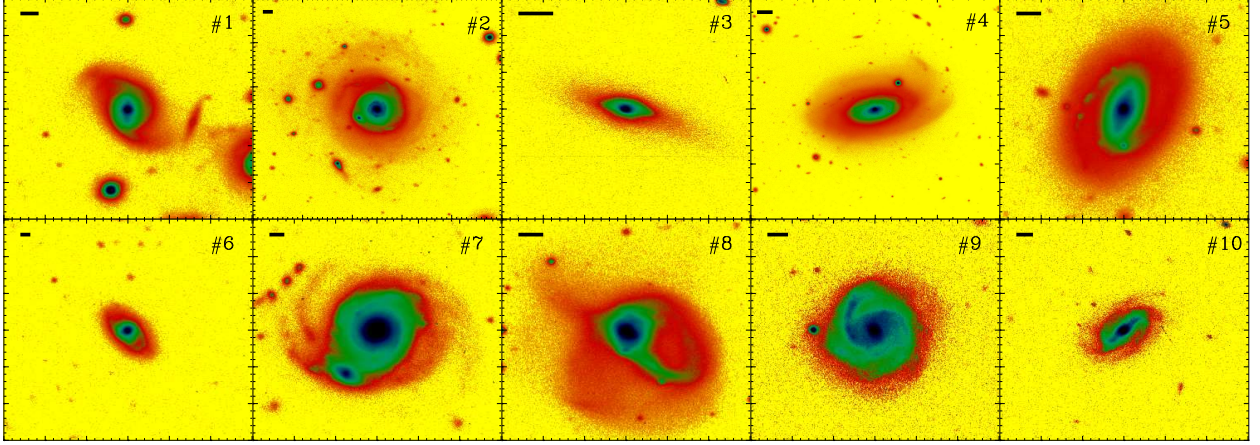


Fig. 1.— *R*-band NOT images of the sample galaxies studied in this work. The pseudo-color images are displayed in logarithmic scale to show up low surface brightness-features. The scale black bar on top left of each image indicates a physical angular separation of 5 kpc. The number on the top right for every image indicates the galaxy ID as in Table 1.

Table 1. Galaxy Sample and Observations

Galaxy #	SDSS ID	Other name	NOT-ALFOSC Date-Obs	Exp-time (s)	Seeing ($''$)
(1)	(2)	(3)	(4)	(5)	(6)
1	J120655.63+501737.1	SBS 1204+505B	Apr-07	2700	1.0
2	J121600.04+124114.3	Mrk 764	May-07	3600	0.7
3	J121607.08+504930.0	Mrk 1469	Apr-07	1700	0.9
4	J141238.14+391836.5	NGC 5515	May-07	3840	0.7
5	J143031.18+524225.8	SBS 1428+529	Apr-07	2400	0.9
6	J144049.35+505009.2	SBS 1439+510	Apr-07	3600	0.9
7	J153810.05+573613.1	SBS 1537+577	Apr-07	4800	1.2
8	J162952.88+242638.3	Mrk883	Apr-07	2400	0.8
9	J212851.19-010412.4	IC 1385	Oct-06	3900	1.0
10	J234428.81+134946.0	...	Oct-06	3600	0.8

Note. — Col. 1: galaxy identification. Col. 2: SDSS ID. Col. 3: other name. Col. 4: observation dates. Col. 5: exposure time. Col. 6: average seeing.

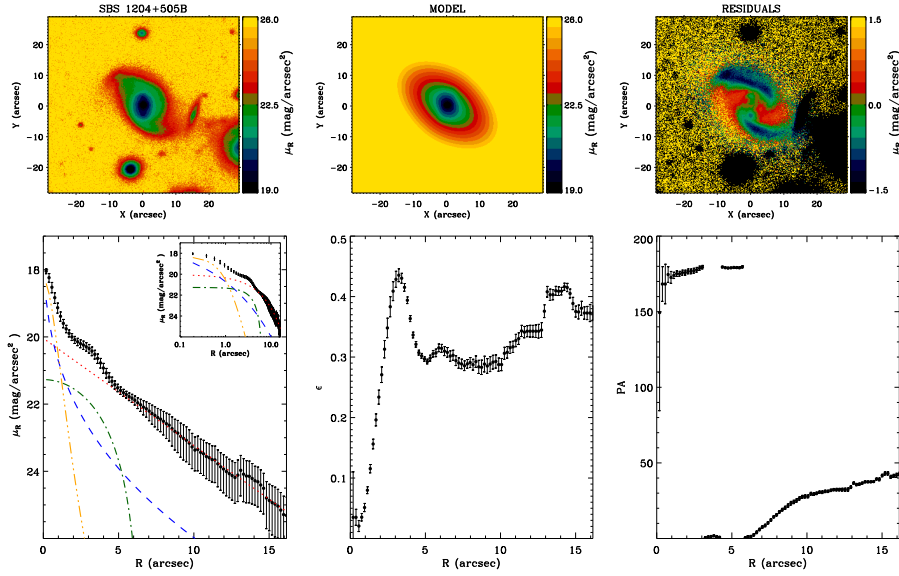


Fig. 2.— *Top left*: NOT image of SDSS J120655.63+501737.1 (SBS 1204+505B) in the R -band. *Top middle*: galaxy model derived from the GASP2D fit considering a central point-like component (fitted with the PSF), a bulge, a bar and a disk component. *Top right*: residuals image derived from the subtraction of the galaxy model from the NOT image. *Bottom left*: surface-brightness distribution of SDSS J120655.63+501737.1. Lines indicate the contribution to the fit of the different components derived with GASP2D: three-dotted-dashed line for the central component, dashed line for the bulge, dotted-dashed line for the bar, and dotted line for the disk. Upper inset shows the fit with a logarithmic scale for the galactocentric distance. *Bottom middle*: ellipticity radial profile measured on the galaxy image. *Bottom right*: position angle (PA) radial profile measured on the galaxy image.

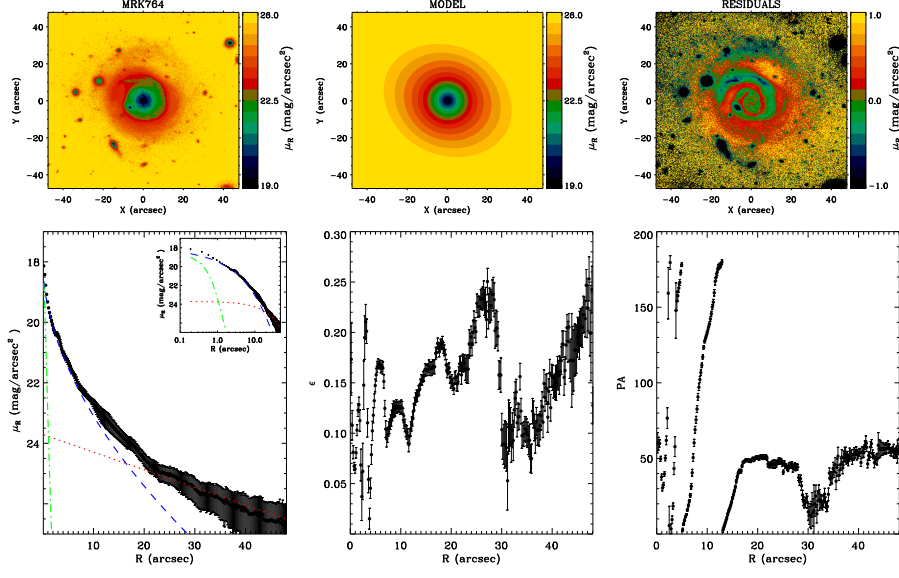


Fig. 3.— J121600.04+124114.3 (#2; Mrk 764). Panel distribution as in Figure 2.

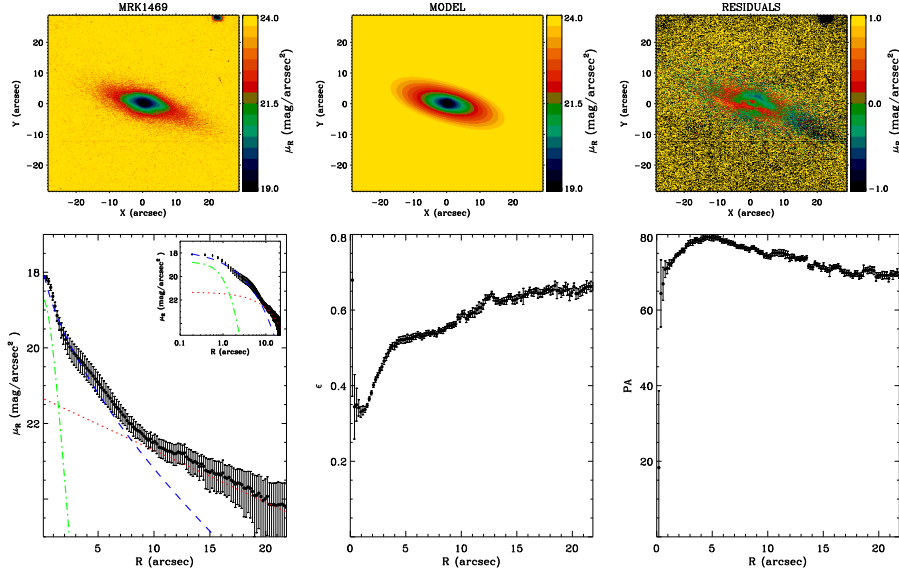


Fig. 4.— J121607.08+504930.0 (#3; Mrk 1469). Panel distribution as in Figure 2.

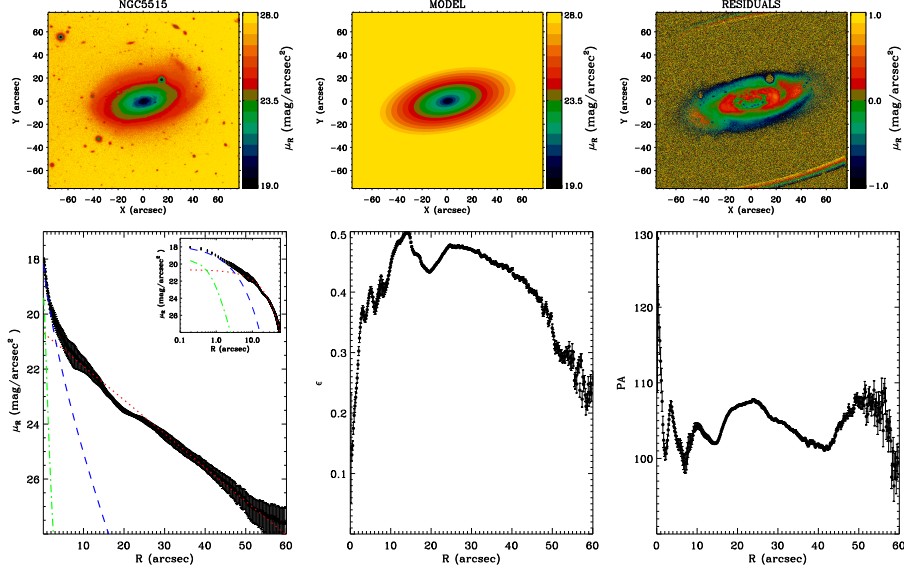


Fig. 5.— J141238.14+391836.5 (#4; NGC 5515). Panel distribution as in Figure 2.

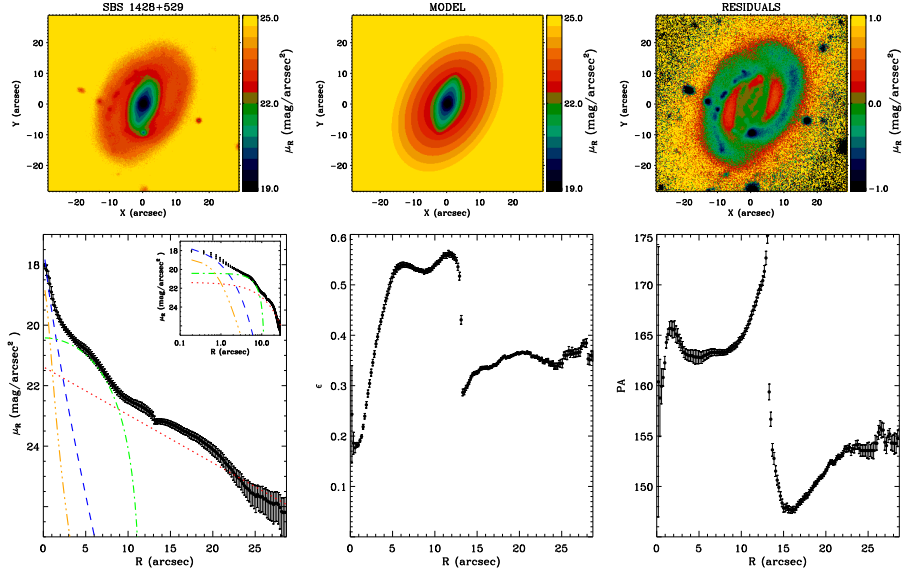


Fig. 6.— J143031.18+524225.8 (#5; SBS 1428+529). Panel distribution as in Figure 2.

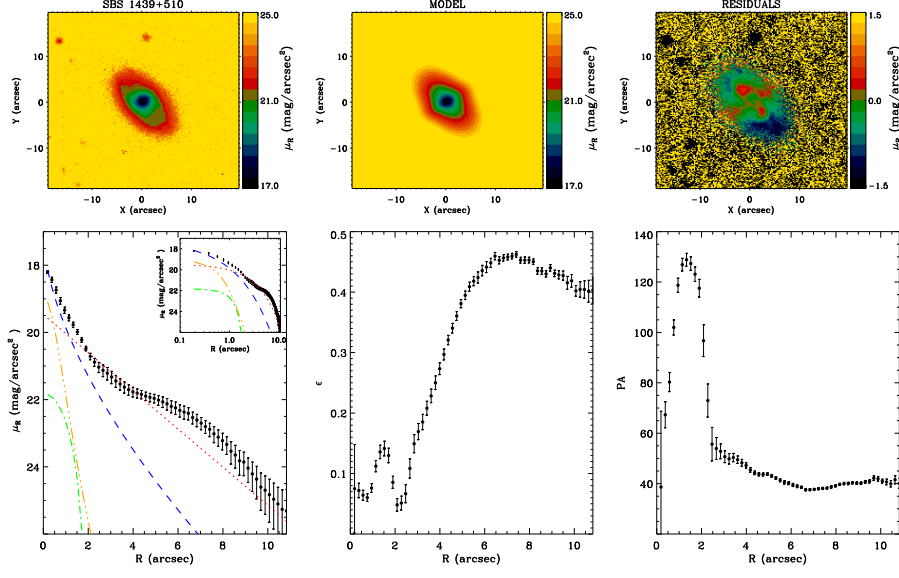


Fig. 7.— J144049.35+505009.2 (#6; SBS 1439+510). Panel distribution as in Figure 2.

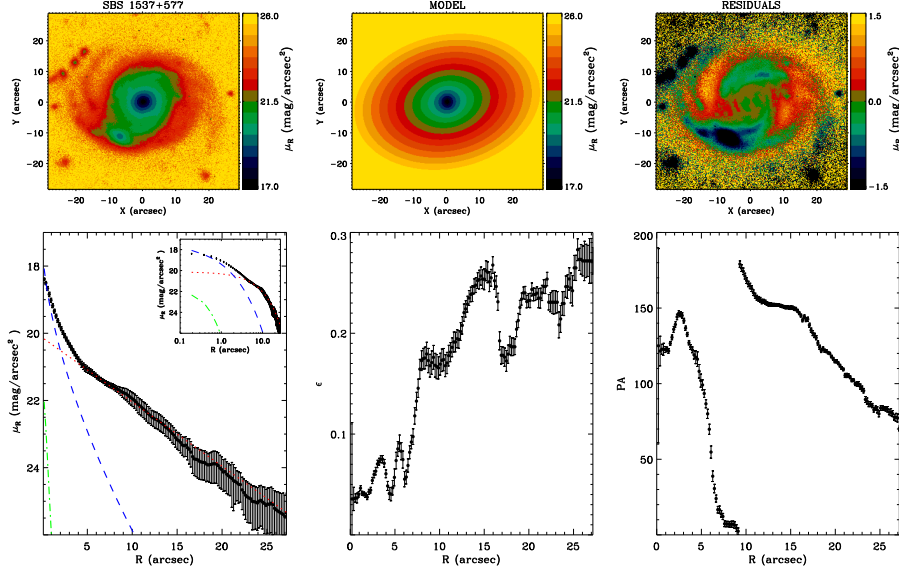


Fig. 8.— J153810.05+573613.1 (#7; SBS 1537+577). Panel distribution as in Figure 2.

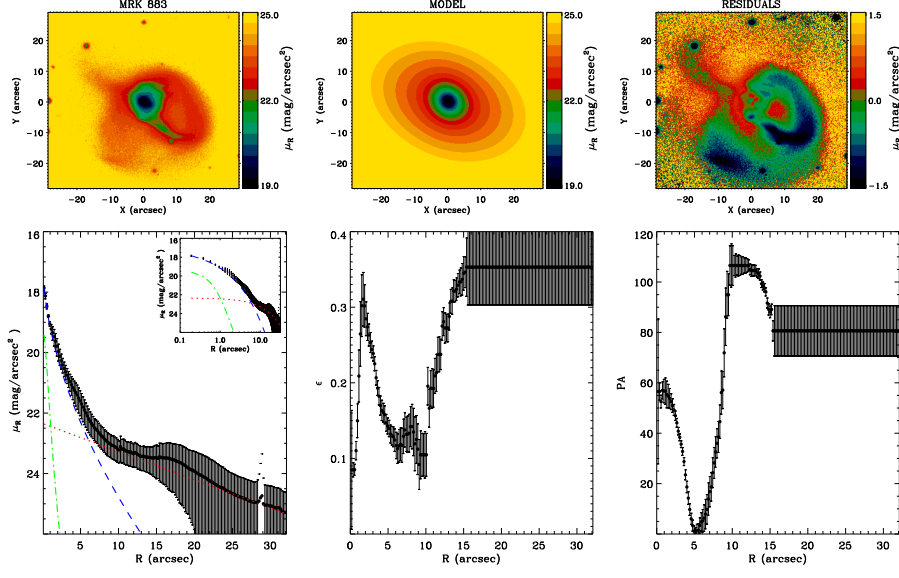


Fig. 9.— J162952.88+242638.3 (#8; Mrk 883). Panel distribution as in Figure 2.

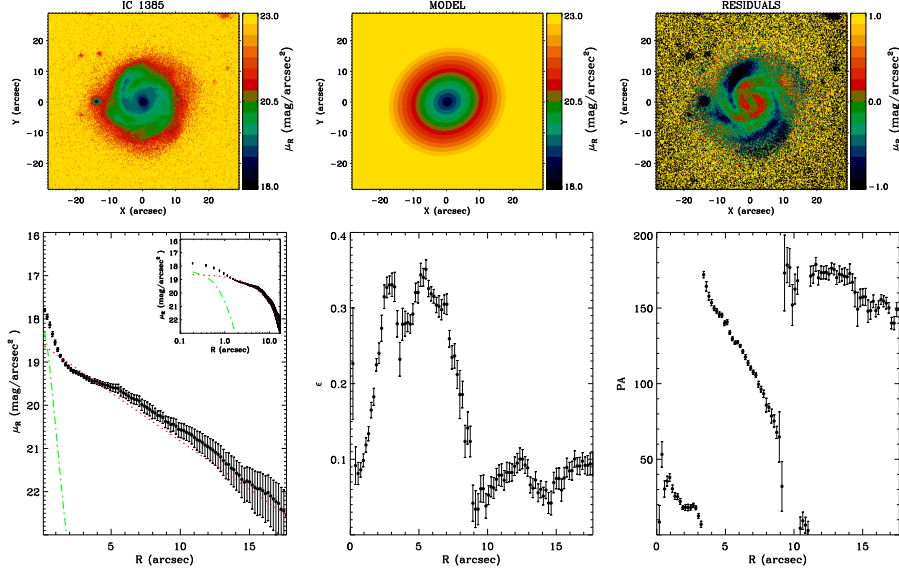


Fig. 10.— J212851.19-010412.4 (#9; IC 1385). Panel distribution as in Figure 2.

Table 2. Host Galaxy Properties **FROM SBD DECOMPOSITION**

Galaxy #	n	r_e h a_{bar}	$(b/a)_{bulge}$ $(b/a)_{disk}$ $(b/a)_{bar}$	$(PA)_{bulge}$ $(PA)_{disk}$ $(PA)_{bar}$	χ^2	Morphological Type	Classical Bulge / Pseudobulge
(1)	(2)	(3)	(4)	(5)	(6)	(7)	(8)
1	2.8 ± 1.2	2.1 ± 0.9 2.8 ± 0.7 5.4 ± 1.6	0.79 ± 0.02 0.59 ± 0.02 0.55 ± 0.02	175.9 ± 1.6 49.6 ± 4.7 0.6 ± 4.2	7.8	SBb **	CB/PB
2	1.8 ± 0.6	4.8 ± 1.1 16.3 ± 1.0 ...	0.95 ± 0.02 0.78 ± 0.01 ...	2.3 ± 3.3 55.6 ± 5.8 ...	4.9	Sb(r)I*	CB/ PB
3	1.6 ± 0.5	1.7 ± 0.4 3.4 ± 0.3 ...	0.34 ± 0.03 0.34 ± 0.01 ...	78.5 ± 2.7 68.8 ± 4.2 ...	3.6	Sb **	PB
4	1.4 ± 0.8	0.9 ± 0.5 3.2 ± 0.2 ...	0.62 ± 0.07 0.48 ± 0.02 ...	102.8 ± 1.5 104.3 ± 2.3 ...	4.1	Sab *	PB
5	1.3 ± 0.6	0.6 ± 0.5 4.7 ± 0.7 7.0 ± 1.3	0.64 ± 0.01 0.63 ± 0.02 0.37 ± 0.02	168.4 ± 2.9 154.4 ± 4.9 164.4 ± 4.7	2.1	SBa-SBab **	PB
6	1.6 ± 0.8	1.9 ± 0.9 2.8 ± 1.4 2.8 ± 3.8	0.49 ± 0.08 0.57 ± 0.03 0.45 ± 0.03	124.7 ± 2.0 40.3 ± 5.1 120.2 ± 3.5	3.5	SBa**	CB/PB
7	1.6 ± 0.3	1.9 ± 0.5 5.4 ± 0.7 ...	0.84 ± 0.02 0.76 ± 0.01 ...	2.3 ± 3.6 105.4 ± 3.5 ...	5.0	Sc**	PB
8	1.8 ± 0.3	1.2 ± 0.4 5.9 ± 0.3 ...	0.83 ± 0.02 0.71 ± 0.01 ...	31.5 ± 3.2 62.3 ± 2.9 ...	6.4	peculiar	uncertain
9 3.3 ± 0.9 0.91 ± 0.02 135.2 ± 6.3	Sab**	uncertain
10	...	0.6 ± 0.5 5.2 ± 0.9	0.80 ± 0.02 0.65 ± 0.02	118.2 ± 3.1 124.8 ± 5.8	3.1	SBab**	uncertain

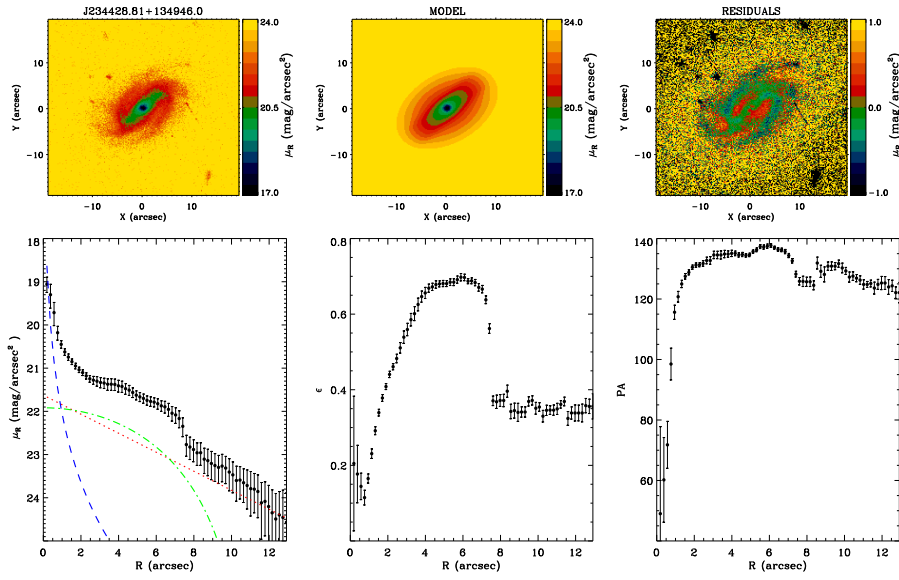


Fig. 11.— J234428.81+134946.0 (#10). Panel distribution as in Figure 2.

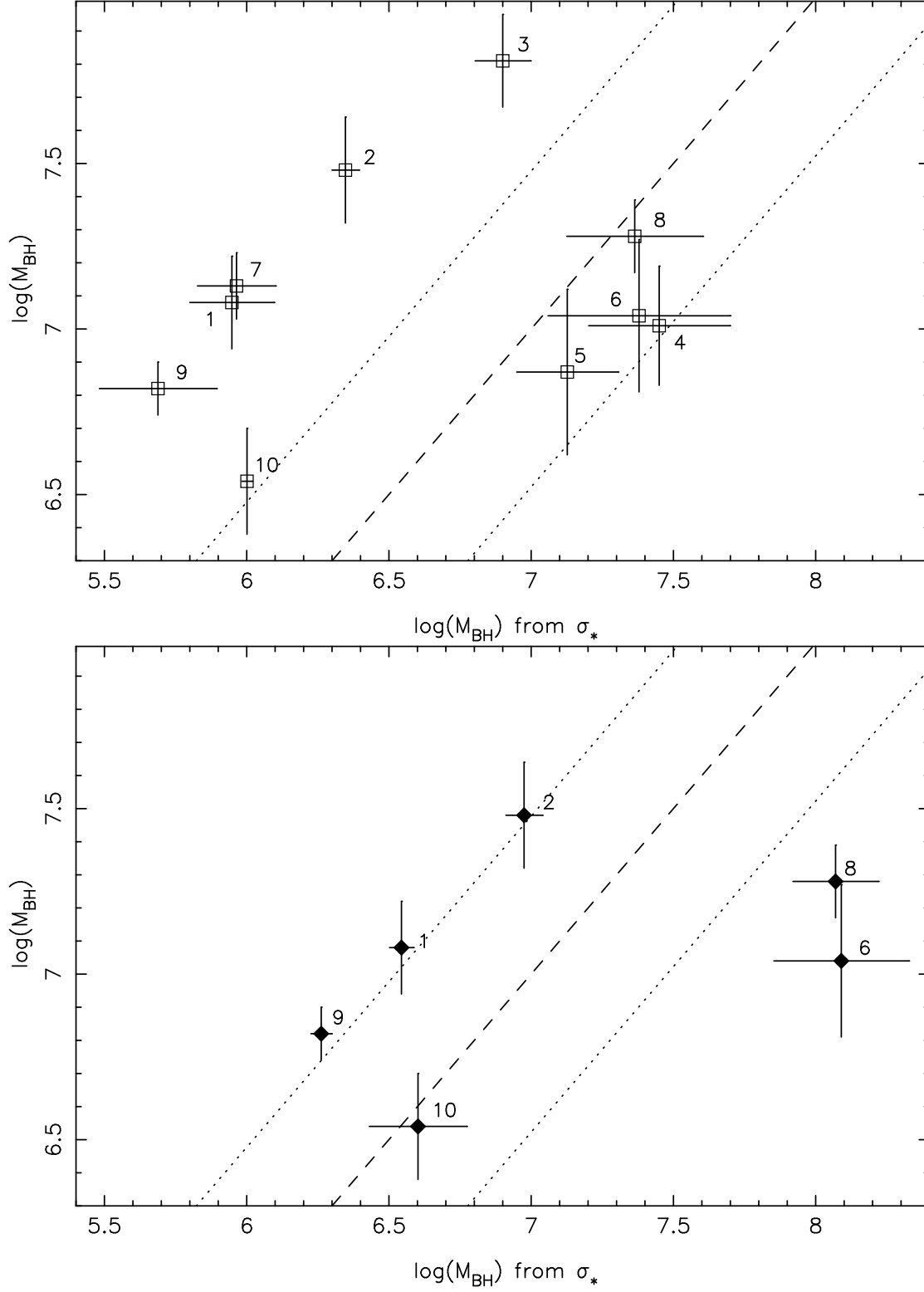


Fig. 12.— *Upper panel:* $M_{\text{BH}}^{\sigma_*}$ derived for pseudobulges using Hu (2008) compared to M_{BH} estimates derived using the scaling relations given by Vestergaard & Peterson (2006). *Lower panel:* $M_{\text{BH}}^{\sigma_*}$ derived for classical bulges using Ferrarese & Ford (2005) compared to M_{BH} , see text.

Table 2—Continued

Galaxy	n	r_e	$(b/a)_{bulge}$	$(PA)_{bulge}$	χ^2	Morphological	Classical Bulge /
#		h	$(b/a)_{disk}$	$(PA)_{disk}$		Type	Pseudobulge
		a_{bar}	$(b/a)_{bar}$	$(PA)_{bar}$			
(1)	(2)	(3)	(4)	(5)	(6)	(7)	(8)
		9.9 ± 1.5	0.30 ± 0.02	133.4 ± 3.7			

Note. — Parameters of the host galaxy derived from the **surface brightness decomposition**, SBD. Col. 1: galaxy # (cf. Table 1). Col. 2: Sérsic index. Col. 3: bulge effective radius in kpc (r_e), disk scale-length in kpc (h), bar length (a_{bar}) in kpc. Col. 4: bulge, disk, and bar axis ratio $(b/a)_{bulge}$, $(b/a)_{disk}$ and $(b/a)_{bar}$, respectively. Col. 5: bulge, disk, and bar position angle $(PA)_{bulge}$, $(PA)_{disk}$ and $(PA)_{bar}$, respectively. Col. 6: χ^2 of the fit. Col. 7: morphology given by NED (*) and derived in this work (**); galaxy 7 is peculiar, probably a merger. Col. 8: host bulge is most probably classical (CB), pseudobulge (PB), or a combination CB/PB.

Table 3. Black Hole Mass Estimates

Galaxy	Morphological	Bulge	$\log M_{\text{BH}}^{\sigma^*}$	$\log M_{\text{BH}}^{\sigma^*}$	$\log M_{\text{BH}}$
	Type	Type	classical bulge	pseudobulge	
#			(M_{\odot})	(M_{\odot})	(M_{\odot})
(1)	(2)	(3)	(4)	(5)	(6)
1	SBb	CB/PB*	6.54±0.04	5.95±0.15	7.08±0.14
2	Sb(r)	CB/ PB	6.97±0.06	6.35±0.05	7.48±0.16
3	Sb	PB*		6.90±0.09	7.81±0.14
4	Sab	PB*		7.45±0.25	7.01±0.18
5	SBa-SBab	PB*		7.13±0.18	6.87±0.25
6	SBa	CB/PB	8.09±0.24	7.38±0.32	7.04±0.23
7	Sc	PB		5.96±0.14	7.13±0.10
8	Peculiar	unknown*	8.07±0.15	7.36±0.24	7.28±0.11
9	Sab	unknown	6.26±0.04	5.69±0.21	6.82±0.08
10	SBab	unknown	6.60±0.17	6.00±0.02	6.54±0.16

Note. — Col. 1: galaxy # (cf. Table 1). Col. 2: morphological classification. Col. 3: classical bulge (CB), pseudobulge (PB). Asterisk indicates objects that display double-peaked emission lines (Paper I). Col. 4: M_{BH} estimates when the host harbors a classical bulge (see Ferrarese & Ford 2005). Col. 5: BH mass estimates when the host harbors a pseudobulge (see Hu 2008). There are 3 objects with bulges showing both possibilities (classical bulge/pseudobulge), thus the M_{BH} mass was estimated using both methods. Col. 6: **BH mass estimates using the scaling relations given by Vestergaard & Peterson (2006) derived in Paper I.**